Electronic Supplementary Material (ESI) for Environmental Science: Nano.
This journal is © The Royal Society of Chemistry 2022

Supporting Information for

Efficient Activation of Peroxymonosulfate by C_3N_5 Doped with Cobalt for Organic Contaminant Degradation

Tai Li[a,b], Peixin Cui[b], Xiaolei Wang[b], Cun Liu[b], Yu Zeng[b], Guodong Fang[*,b], Yuan, Zhao[*,a], Juan Gao[b], Yujun Wang[b], Dongmei Zhou[c]

[a] School of Environmental and Safety Engineering, Changzhou University, Changzhou, 213164, China

[b] Key Laboratory of Soil Environment and Pollution Remediation, Institute of Soil Science, Chinese Academy of Sciences, Nanjing 210008, P.R. China

[c] State Key Laboratory of Pollution Control and Resource Reuse, School of the Environment, Nanjing University, Nanjing 210093, PR China

[*]Corresponding author. Tel.: +86 25 86881607; fax: +86 25 86881000.

E-mail address: gdfang@issas.ac.cn (G.D. Fang)

zhaoyuan12@tsinghua.org.cn (Y. Zhao)

Text S1. Materials

3-Amino-1,2,4-triazde was purchased from Aladdin Bio-Chem Technology Co., LTD (Shanghai, China). Cobalt chloride hexahydrate ($CoCl_2 \cdot 6H_2O$) was obtained from Tianjin Kemio Chemical Reagent Co., Ltd (Tianjin, China). Lithium chloride ($LiCl_2$) was obtained from Macklin Biochemical Technology Co. Ltd. (Shanghai, China).Diethyl phthalate (DEP, >99.9%), sulfamethoxazole (SMX, >98%) and 5, 5-dimethyl-1-pyrroline N-oxide (DMPO, 97%) were supplied by Sigma-Aldrich (USA). Oxone® (peroxymonosulfate, $2KHSO_5 \cdot KHSO_4 \cdot K_2SO_4$) was purchased from Alfa Aesar. Sodium carbonate (Na_2CO_3, 98%), sodium nitrate ($NaNO_3$, 98%), nitrobenzene (NB,99%), Disodium hydrogen phosphate dodecahydrate ($Na_2HPO_4 \bullet 12H_2O$), Sodium phosphate dibasic dihydrate ($NaH_2PO_4 \bullet 2H_2O$), phenol (PhOH, 99%), sodium persulfate ($Na_2S_2O_8$, 98%), sodium hydroxide (NaOH, 97%), sulfuric acid (H_2SO_4, 98%), *tert*-butanol (TBA, 99.5%), and ethanol (EtOH, 99%) were obtained from China National Medicines Corporation Ltd. (Beijing, China). Nitric acid (HNO_3, 98%), Hydrogen peroxide (H_2O_2, 30%), benzoic acid ($C_7H_6O_2$, 99.5%) were supplied by Nanjing Chemical Reagents Co., Ltd. (Nanjing, China). 2,2,6,6-Tetramethyl-4-piperidone (TEMP) and HPLC grade methanol were provided by J&K Scientific Ltd., China (Shanghai).

Text S2

The X-ray absorption fine structure (XAFS) spectra at the Co K-edge of Co-C_3N_5 and references were collected at beamlines BL14W1 and BL11B in Shanghai Synchrotron Radiation Facility (SSRF), with a typical energy of 3.5 GeV and a constant electron current of 220 mA in the storage ring [1]. The focused X-ray was modulated by a Si(111) double-crystal monochromator and calibrated with a Co foil (K-edge at 7709 eV). Co-C_3N_5 and references were positioned at 45° and 90° to the incident X-ray, and the XAFS spectra were gathered in fluorescence and transmission modes, respectively. XAFS data were analyzed with the Demeter software package. The XAFS spectra at the Co K-edge were normalized with Athena, followed by the shell-by-shell fitting with Artemis. The $\chi(k)$ function was wavelet transformed (WT) using the Igor pro script developed by Funke et al The Morlet wavelet was chosen as basis mother wavelet and the parameters (η=6, σ=1) were used for a better resolution in the wave vector k. The k3-weighted Fourier transformed extended x-ray absorption fine structure (EXAFS) spectra were fitted in R-space and the coordination parameters, including the coordination numbers, bond lengths and Debye-Waller factors, were obtained by fitting the theoretical amplitudes to the experimental peaks.

Table S1 XPS analysis of Co-C_3N_5 and other Co-C-N materials reported in the literature (ND means not determined).

Catalyst	Element	Binding energy (eV)	Species	Proportion (%)
Co-C_3N_5	C 1s	283.4	C-N	24.0
		284.8	C-C	38.4
		286.3	C-O	11.0
		288.1	N-C=N	26.6
	N 1s	397.2	Pyridinic N	22.5
		398.5	Pyridinic N-Co	42.0
		399.6	Pyrrolic N	27.1
		401.1	Graphitic N	8.4
	O 1s	530.2	C=O	20.8
		531.2	O-C=O	40.8
		532.7	C-O	38.4
	Co 2p	780.7	Co(II)	37.2
		785.6	Co(III)	28.9
		796.4	Co(II)	17.7
		802.1	Co(III)	16.2
Co-PCN	C 1s	283.9	C-C/C=C	ND
		285.3	C-O	ND
		287.9	N-C=N	ND
	N 1s	397.8	Pyridinic N	7.2
		399.0	Pyrrolic N	2.6
		400.2	Graphitic N	1.7
		402.0	Nitric oxide	ND
	O 1s	530.5	C=O	4.2
		531.4	C-O	6.1
		533.6	O-C=O	0.5
		534.0	Adsorbed oxygen	ND
	Co 2p	777.8	Co(0)	9.4
		780.2	Co-O	10.9
		781.9	Co-Nx	25.9
		785.6	Satellite	ND

Table S2 Comparison of catalytic performances of Co-C_3N_5/PMS and previously reported catalysts in PMS activation and pollutant degradation.

Catalyst	Contaminant	PMS	Performance (%)	Ref.
$LiCoPO_4$ (0.1 g/L)	DEP (5.0 ppm)	0.3 g/L	99 (6 min)	
CuS (1.0 g/L)	DEP (20 ppm)	2.0 mM	65 (120 min)	[2]
Co-C_3N_5 (0.2g/L)	DEP (20 ppm)	2.0 mM	100 (1 min)	This work
Fe-Co-O-C_3N_4 (0.2 g/L)	SMX (0.04 mM)	0.8 mM	100 (30 min)	[3]
Fe-NO-GC (0.1 g/L)	SMX (0.04 mM)	0.4 mM	96.4 (20 min)	[4]
Co-C_3N_5 (0.2 g/L)	SMX (0.4 mM)	2.0 mM	100 (5 min)	This work
Fe-C_3N_4 (0.1 g/L)	4-CP (0.1mM)	1.0 mM	100 (20 min)	[4]
Co_3O_4@MOFs (0.5 g/L)	4-CP (0.78 mM)	0.8 mM	100 (60 min)	[5]
Co-C_3N_5 (0.2 g/L)	4-CP (1.0 mM)	2.0 mM	100 (2 min)	This work
Fe-C_3N_4 (0.1 g/L)	BPA (0.1 mM)	1.0 mM	100 (20 min)	[4]
Fe-MnO_2 (4 g/L)	BPA (5 μM)	0.5 mM	95 (21min)	[6]
Co-C_3N_5 (0.2 g/L)	BPA (1.0 mM)	2.0 mM	100 (5 min)	This work
$CuFe_2O_4$ (0.1 g/L)	PCB28 (0.5 ppm)	0.2 mM	72 (8 h) k_{obs}=0.0082 min^{-1}	[7]
V_2O_3 (0.05 g/L)	PCB28 (1.0 ppm)	2.0 mM	82 (240 min) k_{obs}=0.0169 min^{-1}	[8]
V(V) (0.1 g/L)	PCB28 (1.0 ppm)	2.0 mM	80.1 (48 h) k_{obs}=0.0102 min^{-1}	[9]
MNPs (1.0 g/L)	PCB28 (1.0 ppm)	2.0 mM	90 (240min) k_{obs}=0.0072 min^{-1}	[10]
Co-C_3N_5 (0.2 g/L)	PCB28 (0.5 ppm)	2.0 mM	96 (30 min) k_{obs}=0.1998 min^{-1}	This work

Table S3 EXAFS fitting parameters at the Co K-edge for various samples（S_0^2= 0.776）

Sample	Shell	N^a	R(Å)^b	σ^2(Å^2)^c	ΔE_0(eV)^d	R factor
Co foil	Co-Co	12	2.49	0.0061	6.4	0.0004
CoO	Co-O	6.0	2.06	0.0099	-3.6	0.0004
	Co-Co	12.2	2.99	0.0097		
	Co-O	6.2	3.66	0.0101		
CoPc	Co-N	4.0	1.91	0.0016	6.8	0.0025
Co-C_3N_5	Co-N	4.1	2.06	0.0020	0.7	0.0002
Co-C_3N_5 after PMS activation	Co-N	4.0	2.06	0.0013	0.5	0.0001

$^a N$: coordination numbers; $^b R$: bond distance; $^c \sigma^2$: Debye-Waller factors; ^{d} ΔE_0: the inner potential correction. R factor: goodness of fit. S_0^2 was set to 0.776 for Co, according to the experimental EXAFS fit of Co foil references by fixing CN as the known crystallographic value.

Table S4 GC-MS retention times (Rt), possible structures, and EI mass spectra of TMS derivatives of the intermediates from PCB28 degradation in the Co-C_3N_5/PMS system.

Intermediates number	*Rt* (min)	Possible structure	Mass spectra (TMS derivatives)
1	8.25	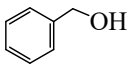	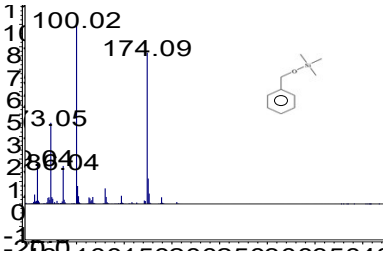
2	10.46	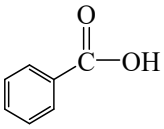	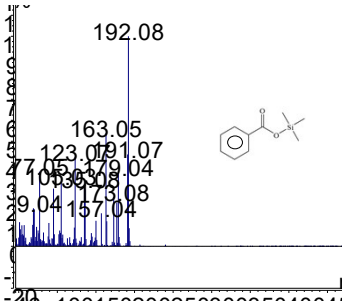
3	21.05	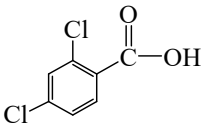	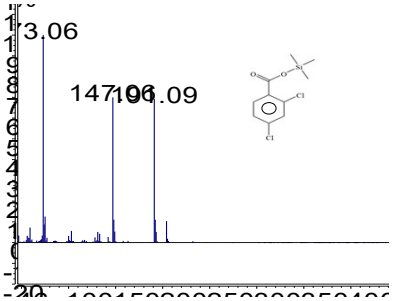
4	25.06	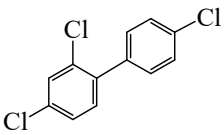	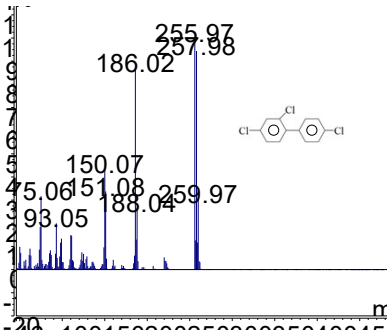

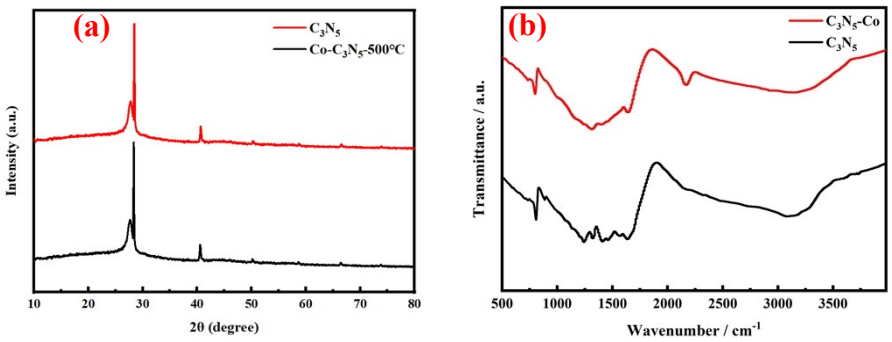

Figure S1. Characterizations of C_3N_5 and Co-C_3N_5: (a) XRD pattern; (b) FTIR of C_3N_5 and Co-C_3N_5.

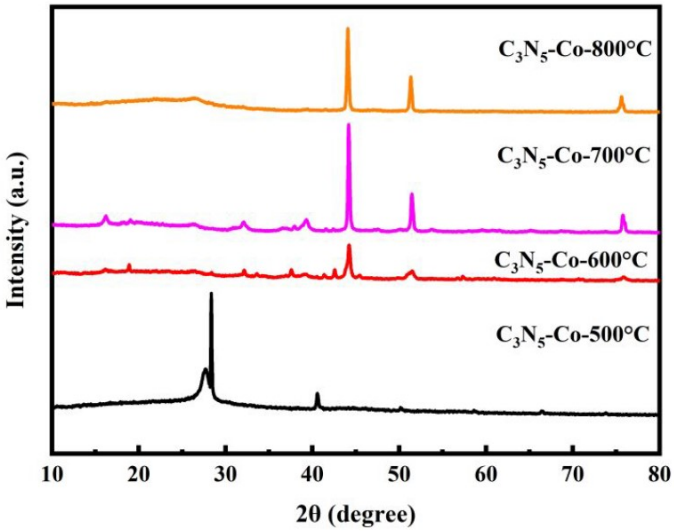

Figure S2. XRD patterns of Co-C_3N_5 synthesized at different temperatures

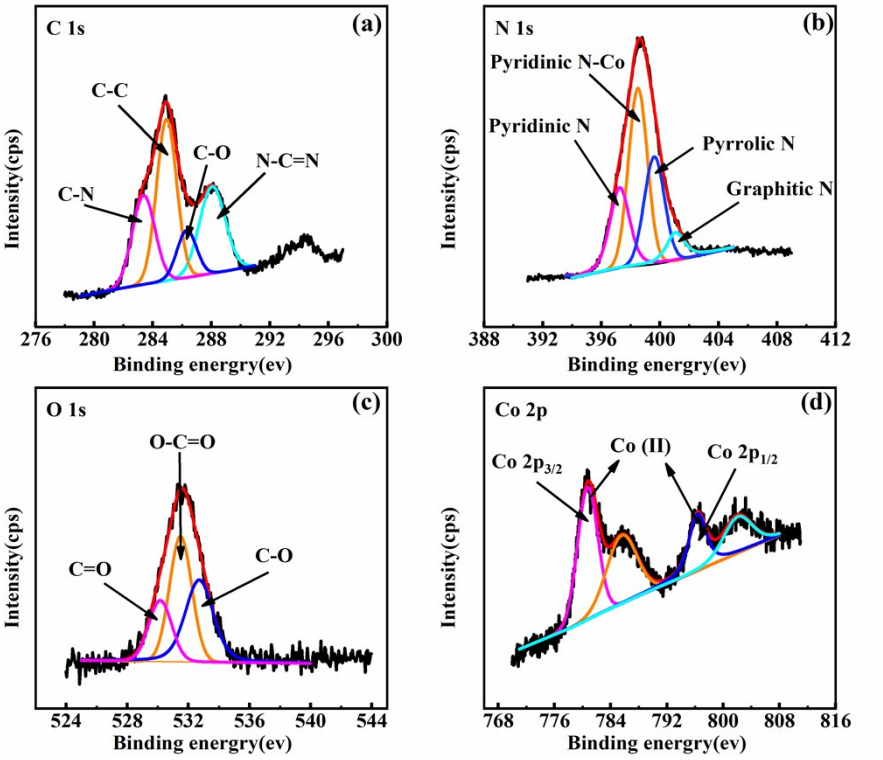

Figure S3. XPS spectra of Co-C_3N_5 at 500°C with Co ratio of 3 wt%: (a) C 1s, (b) N 1s, (c) O 1s, (d) Co 2p.

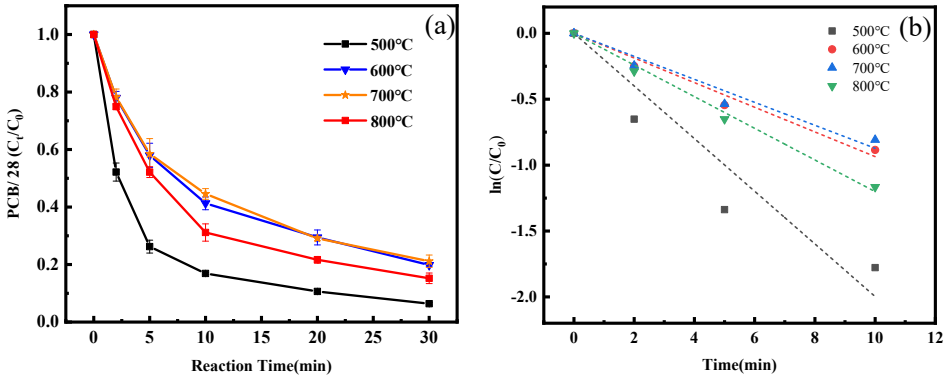

Figure S4. PMS activation by Co-C_3N_5 for PCB28 degradation: (a) kinetics of PCB28 degradation with Co-C_3N_5 calcined at different temperatures; (b) first-order kinetics fitting. Reaction conditions: $[PCB28]_0$ = 0.5 mg/L, $[PMS]_0$ = 0.8 mM, [Co-C_3N_5] = 0.2 g/L, 25 °C, pH = 7.0.

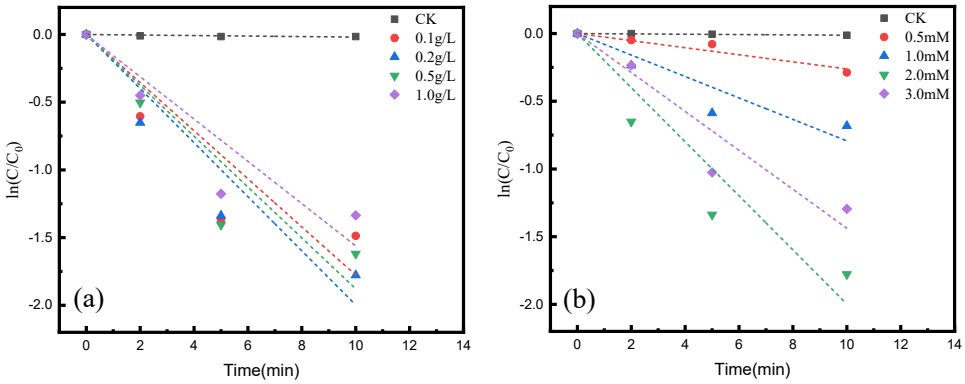

Figure S5. The pseudo-first-order kinetic fitting on different Co-C_3N_5 loading (a) and PMS concentration (b). Reaction conditions: $[Co\text{-}C_3N_5]_0$ =0–1.0 g/L, $[PCB28]_0$ = 0.5 mg/L, $[PMS]_0$ = 0.5–3.0 mM, initial pH = 3.0-11.0 (buffer solution) and 25 °C.

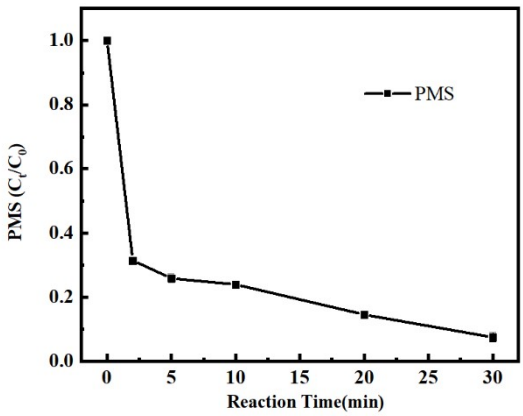

Figure S6. Kinetics of PMS decomposition by Co-C_3N_5 (500°C) during the PCB28 degradation. Reaction conditions: $[PCB28]_0$ = 0.5 mg/L, $[PMS]_0$ = 0.8 mM, [Co-C_3N_5] = 0.2 g/L, 25 °C, pH = 7.0.

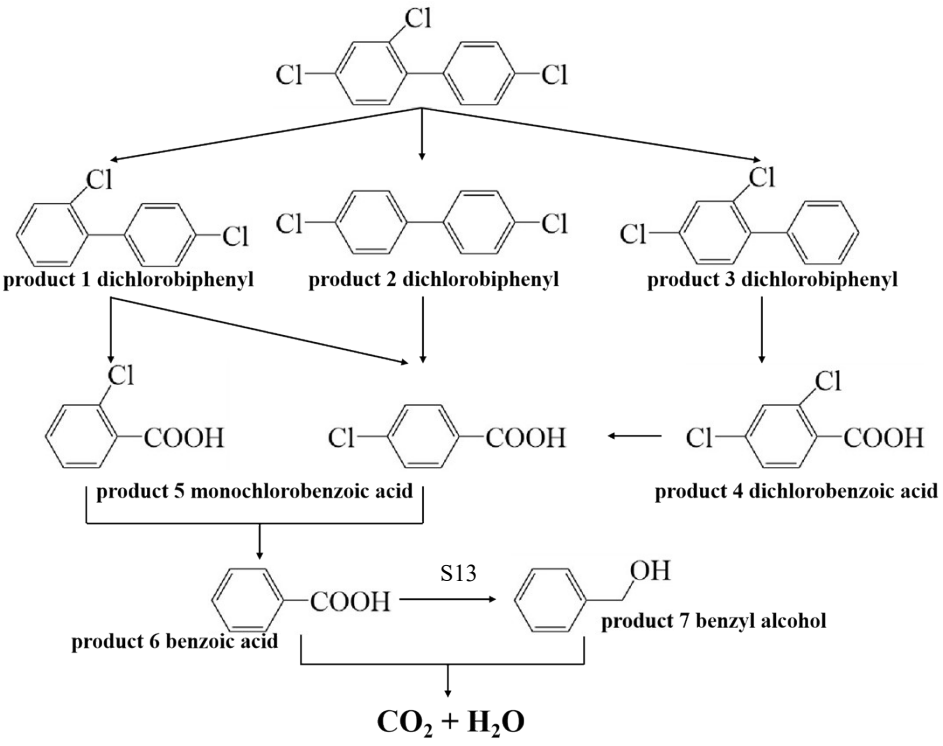

Figure S7. Proposed pathway of PCB28 degradation in the Co-C_3N_5/PMS system.

References

[1] H. Funke, A.C. Scheinost, M. Chukalina, Wavelet analysis of extended x-ray absorption fine structure data, Physical Review B, 71 (2005).
[2] X.L. Wang, Y.Z. Ding, D.D. Dionysiou, C. Liu, Y.P. Tong, J. Gao, G.D. Fang, D.M. Zhou, Efficient activation of peroxymonosulfate by copper sulfide for diethyl phthalate degradation: Performance, radical generation and mechanism, Science of the Total Environment, 749 (2020).
[3] S.Z. Wang, Y. Liu, J.L. Wang, Peroxymonosulfate Activation by Fe-Co-O-Codoped Graphite Carbon Nitride for Degradation of Sulfamethoxazole, Environmental Science & Technology, 54 (2020) 10361-10369.
[4] H.C. Li, C. Shan, B.C. Pan, Fe(III)-Doped g-C3N4 Mediated Peroxymonosulfate Activation for Selective Degradation of Phenolic Compounds via High-Valent Iron-Oxo Species, Environmental Science & Technology, 52 (2018) 2197-2205.
[5] T. Zeng, X.L. Zhang, S.H. Wang, H.Y. Niu, Y.Q. Cai, Spatial Confinement of a Co3O4 Catalyst in Hollow Metal-Organic Frameworks as a Nanoreactor for Improved Degradation of Organic Pollutants, Environmental Science & Technology, 49 (2015) 2350-2357.
[6] K.Z. Huang, H.C. Zhang, Direct Electron-Transfer-Based Peroxymonosulfate Activation by Iron-Doped Manganese Oxide (delta-MnO2) and the Development of Galvanic Oxidation Processes (GOPs), Environmental Science & Technology, 53 (2019) 12610-12620.
[7] W.X. Qin, G.D. Fang, Y.J. Wang, D.M. Zhou, Mechanistic understanding of polychlorinated biphenyls degradation by peroxymonosulfate activated with CuFe2O4 nanoparticles: Key role of superoxide radicals, Chemical Engineering Journal, 348 (2018) 526-534.
[8] G.D. Fang, W.H. Wu, C. Liu, D.D. Dionysiou, Y.M. Deng, D.M. Zhou, Activation of persulfate with vanadium species for PCBs degradation: A mechanistic study, Applied Catalysis B-Environmental, 202 (2017) 1-11.
[9] G.D. Fang, W.H. Wu, Y.M. Deng, D.M. Zhou, Homogenous activation of persulfate by different species of vanadium ions for PCBs degradation, Chemical Engineering Journal, 323 (2017) 84-95.
[10] G.D. Fang, D.D. Dionysiou, S.R. Al-Abed, D.M. Zhou, Superoxide radical driving the activation of persulfate by magnetite nanoparticles: Implications for the degradation of PCBs, Applied Catalysis B-Environmental, 129 (2013) 325-332.